JOURNAL OF SPACECRAFT AND ROCKETS
Vol. 44, No. 6, November–December 2007

Assessment of Two Low-Reynolds-Number k-ε Models in Turbulent Boundary Layers with Surface Roughness

Meng-Huang Lu and William W. Liou
Western Michigan University, Kalamazoo, Michigan 49008

DOI: 10.2514/1.30738

The performance of two low-Reynolds-number k-ε models developed for flows over rough walls is assessed by simulating the fully developed turbulent flows in rough circular pipes, in rough rectangular channels, and over rough flat plates. The computational results, including the log-law mean velocity, the skin friction coefficient, the roughness function, the turbulent kinetic energy, and the Reynolds shear stress, are presented. For the turbulent rough-pipe and rough-channel flows calculated, the results show various levels of agreement with measured data for both models. For the turbulent boundary layer, the results obtained by using one of the models agree satisfactorily with the measured log-law mean velocity profiles and roughness functions. Both models less satisfactorily predict the skin friction coefficient and the turbulent kinetic energy.

Nomenclature

C_f	=	skin friction coefficient
D	=	hydraulic diameter
H	=	channel height
k	=	turbulent kinetic energy
k_s	=	roughness height
k_{eq}	=	equivalent sand roughness height
k^+	=	normalized turbulent kinetic energy, k/u_τ^2
k_{eq}^+	=	normalized equivalent sand roughness height, $u_\tau k_{eq}/\nu$
k_s^+	=	normalized roughness height, $u_\tau k_s/\nu$
Re	=	Reynolds number
Re_θ	=	Reynolds number based on momentum thickness
R_t	=	turbulent Reynolds number, $k^2/\varepsilon\nu$
t	=	time
U	=	mean velocity
U_e	=	edge velocity
U^+	=	normalized velocity, U/u_τ
u_τ	=	friction velocity
$-uv$	=	Reynolds shear stress
$-u^+v^+$	=	normalized Reynolds shear stress, $-uv/u_\tau^2$
W	=	channel width
y	=	normal distance from the wall
y^+	=	normalized distance from the wall, $u_\tau y/\nu$
ΔU^+	=	roughness function
δ	=	boundary-layer thickness
ε	=	dissipation rate of turbulent kinetic energy
θ	=	momentum thickness
ν	=	kinematic viscosity

I. Introduction

TURBULENT boundary layers developed over rough surfaces occur in a wide range of flows, such as boundary layers over naval vehicle platforms, flight vehicles, turbomachinery blades, pipes, and heat exchangers. They present great challenges and interests in engineering. Surface roughness influences the flow structures in the turbulent boundary layers and can cause the increase of drag and wall heat transfer [1], which greatly affect the design of the thermal protection system for spacecraft and hypersonic reentry vehicles. The effect of surface roughness has been considered in many experimental studies since Nikuradse [2].

Several reviews on the turbulent boundary layers over rough walls can be found in the literature [3–5]. Clauser [6,7] and Hama [8] suggested that the effect of surface roughness on the mean flow was confined to the inner layer, causing an increase of the skin friction and the lowering of the log-law mean velocity profile, compared with that for smooth walls. This log-law velocity downward shift is referred to as the roughness function ΔU^+ for k-type roughness, such as sand grains and two-dimensional rods [9]. The roughness function ΔU^+ for k-type roughness has been found to vary with the Reynolds number based on the shear velocity and has been correlated to the equivalent sand roughness k_{eq}^+. Clauser [6,7] and Hama [8] also found that the velocity defect form of the mean velocity in the outer region is independent of surface roughness. Many other measurements [3,10–13] have provided support to the universality of the velocity defect law. The collapse of the mean velocity defect profiles for rough and smooth walls is consistent with the wall similarity hypothesis of Townsend [14], stating that the rough-wall and smooth-wall boundary layers would have the same turbulence structures in the core part of the boundary layer at sufficiently high Reynolds numbers. Schultz and Flack [11,12] and Flack et al. [13] measured the turbulent boundary layers over flat plates with different k-type surface roughness, including packed uniform spheres, sandpaper, and woven meshes. The results of these studies support Townsend's wall similarity hypothesis. However, there are also measurements that suggest otherwise [15–20]. Krogstad et al. [16] and Krogstad and Antonia [17,18] conducted a series of works on comparing zero-pressure-gradient turbulent boundary layers over the surface roughness of two-dimensional rods and three-dimensional mesh screens. Keirsbulck et al. [19] measured zero-pressure-gradient turbulent boundary layers over the rough wall of two-dimensional square bars. Their results show that the surface roughness changes the profile of the velocity defect in the inner region, which results in a higher degree of isotropy of the Reynolds normal stresses and modifies the Reynolds shear stress profiles in the outer region of the boundary layer. This indicates that the interaction of the inner and outer regions of the turbulent boundary layers over rough surfaces may be important in some cases.

Surface roughness also poses a major challenge to numerical simulations [21]. Numerical studies of surface roughness have been performed using direct numerical simulation (DNS), large eddy simulation (LES), and the Reynolds-averaged Navier–Stokes (RANS) equations, and in the form of correlations [22–24]. There are two commonly used methods in DNS and LES to simulate the effect

Presented as Paper 1448 at the 45th AIAA Aerospace Sciences Meeting and Exhibit, Reno, NV, 8–11 January 2007; received 28 February 2007; accepted for publication 3 August 2007.

*Graduate Assistant, Mechanical and Aeronautical Engineering.
†Professor, Mechanical and Aeronautical Engineering. Senior Member AIAA.

of surface roughness. The first approach is to account for the blockage effect of the roughness element on the flow by adding a form-drag term in the momentum equation [25–28]. The coefficient for the form-drag term is determined a priori by examining the corresponding experimental data. The second is the body force/immersed boundary method [29–32], in which the no-slip boundary is prescribed as a body force obtained during the numerical solution. For the numerical calculation using RANS, the effect of the surface roughness is modeled. One commonly used approach is adding form-drag terms in the governing equations to account for the roughness effect [33–38]. However, the coefficients in the formulations for the form drag are flow-specific and are set with a detailed knowledge of the shape and distribution of the roughness elements, which are not readily obtainable in most engineering applications. RANS-based calculations have also been performed by using roughness models that are adapted from the existing turbulence models developed for smooth walls. Krogstad [39] modified the damping function of van Driest [40] to reproduce the roughness function variation for large roughness. For Reynolds numbers between 10^5 to 10^7, Youn et al. [41] employed the standard k-ε model with a wall function to predict the friction factor for flows in rectangular ducts that are roughened on one side of the duct with ribs. The rib height varies from 0.01 to 0.04 of the hydraulic diameter of the duct, and the distance between ribs varies from 10 to 40 times the rib height.

A common approach adopted in the numerical modeling of roughness is to relate the roughness effects to an equivalent sand roughness, thereby ignoring any possible dependency of the turbulent flow structure on the specific surface geometry. Zhang et al. [42] proposed a new low-Reynolds-number k-ε model to simulate turbulent flow over smooth and rough surfaces by including the equivalent sand roughness height into the damping functions of van Driest [40], and Lam and Bremhorst [43]. The results in Zhang et al. [42] show that the skin friction coefficient and the log-law velocity shift agree well with the experimental measurements of fully developed rough pipe and duct flows of Reynolds numbers between 5×10^3 and 5×10^7 and roughness heights k_{eq}^+ from 0 up to 1000. Durbin et al. [44] added a hydrodynamic roughness length to the two-layer k-ε turbulence model of Chen and Patel [45] for the sand-grain roughness surface. The numerical formulation was validated for flat-plate boundary layers with accelerated freestream and the flows over a backward-facing ramp. Foti and Scandura [46] developed a new low-Reynolds-number k-ε model for oscillatory flows over smooth and rough surfaces based on the smooth-wall turbulence model of Lam and Bremhorst [43]. The results [46] show that the model well predicts the wall shear stress, mean velocity profiles, and boundary-layer thickness for steady and oscillatory flows over a wavy sea bed.

The low-Reynolds-number k-ε models of Zhang et al. [42] and Foti and Scandura [46] are applied in this study. The roughness modeling terms in both models involve only the equivalent sand-grain roughness and contain no model coefficients that depend on the roughness geometry. The model of Zhang et al. [42] has been shown to well predict the rough-wall log-law mean velocity profiles and the wall shear stress in rough pipes and channels. However, results for turbulence properties have not been reported and the model has not been applied to turbulent boundary-layer flows over rough plates. The model of Foti and Scandura [46] has been validated for oscillatory flows over a wavy sea bed. Their model has not been applied to other types of rough surfaces.

In this paper, the two roughness models are applied to turbulent flows in rough circular pipes, in rough rectangular channels, and over rough flat plates. The results of these calculations, and their comparisons with the corresponding measured data, are presented and discussed. We focus on the k-type surface roughness because both models have been calibrated with measurements for k-type surface roughness. The performance of these two models is first evaluated by calculating the turbulent flows in these geometries with smooth walls and comparing the results with the corresponding measurements and DNS data [47–49]. The fully developed turbulent rough-pipe and rough-channel flows are then calculated and the numerical results are compared with the experimental data. For the turbulent boundary layers over flat plates, different types of surface roughness, including uniform spheres [12], sandpaper [13], and mesh screens [10,13], are numerically studied and the results are compared with the corresponding experimental data.

In the following sections, the details of turbulence models and numerical methods used in this study are presented. These are followed by a Results and Discussion section, in which the simulation results obtained are presented, compared, and discussed.

II. Turbulence Models

The nondimensional incompressible forms of the transport equations for k and ε for the two low-Reynolds-number k-ε models studied can be written in a generalized curvilinear coordinates system ξ^k as follows:

$$\frac{\partial k}{\partial t} + V^j \frac{\partial k}{\partial \xi^j} = J \frac{\partial}{\partial \xi^j} \left\{ \left(\frac{1}{Re} + \frac{\nu_t}{\sigma_k} \right) \frac{g^{jp}}{J} \frac{\partial k}{\partial \xi^p} \right\} + G - \varepsilon \tag{1}$$

$$\frac{\partial \varepsilon}{\partial t} + V^j \frac{\partial \varepsilon}{\partial \xi^j} = J \frac{\partial}{\partial \xi^j} \left\{ \left(\frac{1}{Re} + \frac{\nu_t}{\sigma_\varepsilon} \right) \frac{g^{jp}}{J} \frac{\partial \varepsilon}{\partial \xi^p} \right\} + C_1 f_1 \frac{\varepsilon}{k} G - C_2 f_2 \frac{\varepsilon^2}{k} \tag{2}$$

$$\nu_t = C_\mu f_\mu \frac{k^2}{\varepsilon} \tag{3}$$

where J denotes the Jacobian of the geometric transformation, and g^{jp} represents the contravariant metric tensor of the geometric transformation, defined as

$$g^{jp} = \xi^j_{x_i} \xi^p_{x_i} \tag{4}$$

$$\xi^j_{x_i} = \frac{\partial \xi^k}{\partial x_i} \tag{5}$$

where x_i denotes the Cartesian coordinates, and V^j are the contravariant components of the mean Cartesian velocity components U_k, defined as

$$V^j = U_k \xi^j_{x_k} \tag{6}$$

The first terms on the right-hand side of Eqs. (1) and (2) are the diffusion terms, and the last two terms represent production and dissipation terms. The production term G can be expressed as follows:

$$G = \frac{1}{2} \nu_t \left(\frac{\partial U_i}{\partial \xi^k} \xi^k_{x_j} + \frac{\partial U_j}{\partial \xi^k} \xi^k_{x_i} \right)^2 \tag{7}$$

where σ_k, σ_ε, C_1, C_2, and C_μ are model constants. For both models, the values of these model constants are the same as those used in the standard k-ε model. That is, $\sigma_k = 1.0$, $\sigma_\varepsilon = 1.3$, $C_1 = 1.44$, $C_2 = 1.92$, and $C_\mu = 0.09$.

The difference between the two models appears mainly in the form of the damping functions. The damping functions f_μ, f_1, and f_2 proposed by Zhang et al. [42] are described as follows:

$$f_\mu = 1 - \exp[-(y^+/42)^2] + f_{\mu,s} \tag{8}$$

$$f_{\mu,s} = g_1\left(k_{\text{eq}}^+\right) \exp\left(-25y^+/k_{\text{eq}}^+\right) \tag{9}$$

$$f_1 = 1 + g_2\left(k_{\text{eq}}^+\right)[9.2/(1 + y^+)]^6 \tag{10}$$

$$f_2 = 1 - \exp\left(-R_t^2\right) \tag{11}$$

For a smooth wall, $g_1(k_{eq}^+) = 0$ and $g_2(k_{eq}^+) = 1$. For a rough wall, the extent of the viscous region is reduced due to the enhanced turbulent mixing. This roughness effect is achieved in Zhang et al. [42] by including an additional term $f_{\mu,s}$ to the formulation of the model damping function f_μ with a positive-definite roughness modeling function $g_1(k_{eq}^+)$. It was also argued that the value of f_1 for rough-wall modeling should be lower than that used for smooth-wall modeling in the near-wall region due to the reduced production of the rate of dissipation ε. Therefore, a second roughness modeling function $g_2(k_{eq}^+)$ is used; $g_2(k_{eq}^+) = 1$ for a smooth wall ($k_{eq}^+ = 0$) and decreases with increasing k_{eq}^+. The expressions of the roughness modeling functions are

$$g_1(k_{eq}^+) = \sqrt{k_{eq}^+/200} \tag{12}$$

$$g_2(k_{eq}^+) = \exp\left[-1/\left(0.1 + 1/k_{eq}^+\right)\right] \tag{13}$$

For the low-Reynolds-number k-ε model of Foti and Scandura [46], the damping functions have the following forms:

$$f_\mu = [1 - \exp(-0.0160R_k)]^2(1 + 20.5/R_t) + f_{\mu,s} \tag{14}$$

$$f_{\mu,s} = S\{1.0 - \tanh[0.15(y^+ - 5.0S)/S]\} \tag{15}$$

$$f_1 = 1 + (0.05/f_\mu)^3 \tag{16}$$

$$f_2 = 1 - \exp\left(-R_t^2\right)/\left(1 + 0.01k_{eq}^+\right) \tag{17}$$

where $R_k = k^{1/2}y/\nu$, and S is a function of the equivalent sand roughness k_{eq}^+. The value of S is determined through a calibration with experimental data [50]. Similar to the model of Zhang et al. [42], the modification to damping function f_μ is to obtain the effect of increased turbulent mixing near the rough wall. The damping function f_2 is modified to further decrease the sink terms in the dissipation rate equation.

In general, both of the models studied here adapt the forms of the damping functions found in existing low-Reynolds-number k-ε models developed for a smooth wall by including roughness correction functions. The roughness effects are modeled through the use of the equivalent sand-grain roughness k_{eq}^+ and are not shape-dependent. For the cases here, the equivalent sand-grain roughness is provided by their corresponding experimental studies.

III. Numerical Methods

The numerical method used in this study solves the three-dimensional RANS equations in the generalized curvilinear coordinates. The velocity components are expressed in Cartesian coordinates, following a partial transformation approach. The governing equations are discretized in space on a nonstaggered grid using second-order approximations. The convective terms in the momentum equations are discretized by using second-order-accurate upwind differencing. The pressure gradient and viscous terms in the momentum equations and the divergence operator in the continuity equation are discretized by second-order-accurate central finite differencing. A discrete pressure-Poisson equation is used to enforce the incompressibility constraint. The formulation of Sotiropoulos and Abdallah [51], designed to avoid the odd–even decoupling inherent in the case of nonstaggered grids, was adopted.

The discrete momentum equations are integrated in time using a four-stage explicit Runge–Kutta scheme. The pressure-velocity equation is solved using the alternate-direction-implicit approximate factorization method, to accelerate its convergence, and the Thomas algorithm. The pressure-Poisson equation is transformed into a diffusionlike evolution equation. Convergence acceleration techniques such as local time stepping and implicit residual smoothing are used to enhance the error damping properties of the time-marching procedure. This numerical methodology has been tested for a wide range of laminar flows and turbulent flows with various turbulence closures [52–55]. The comparisons of the computed solutions with other numerical results and experimental data demonstrated their ability to simulate those flows with great accuracy. The turbulence model transport equations (1) and (2) are discretized in space and integrated in time following a similar procedure to that indicated earlier for the momentum equations for the mean flow. A four-stage Runge–Kutta method is also used to advance the discrete equations in time.

A. Computational Domains

In this study, the axisymmetric solutions for pipe flows and two-dimensional solutions for channels and flat plates are sought. The computational domain for the fully developed turbulent smooth and rough-pipe flows extends 150 pipe diameters downstream, and only a quarter of the pipe was simulated. For the fully developed turbulent smooth and rough-channel flows, the domain extends 150 channel heights downstream, and only a half of the channel was simulated. For the turbulent boundary layers over smooth and rough plates, the value of y^+ for the first grid point away from the wall is less than 0.1, and a hyperbolic tangent stretching function was used in the wall-normal direction with a grid clustered in the near-wall region.

B. Boundary Conditions

The boundary conditions were specified as follows. The inlet boundary conditions for the fully developed turbulent smooth pipe and smooth channel flows are assumed uniform for all variables, where $U = 1$, $V = W = 0$, and $k = \varepsilon = 10^{-6}$. For the smooth flat plates, the Blasius solution was used at the inlet with uniform profiles of $k = 0.013$ and $\varepsilon = 7$ [56]. The smooth-wall solutions thus obtained are then used to initialize the corresponding rough-wall calculations. On the symmetry boundaries, the mirror-image reflections for the grid and the flow variables are used for the fully developed turbulent smooth and rough pipe and channel flows. For all cases, the exit boundary condition is imposed by assuming zero streamwise diffusion. At the outer boundary of the flat plate, the turbulent boundary layer assumes the corresponding freestream conditions. The wall boundary condition is zero value for the three velocity components and the turbulent kinetic energy, and $\varepsilon = 1/Re(\partial^2 k/\partial y^2)$. However, the second-order derivative does not always guarantee a positive value for the dissipation rate of turbulent kinetic energy at the wall. It has been proposed [57] to employ $\varepsilon = 2/Re(k_1/y_1^2)$ as an approximation to the value of ε at the wall, where the subscript 1 denotes the nearest grid point from the wall.

C. Grid-Independence Study

For the pipe flows, the numerical grid in the radial direction is generated by using a hyperbolic stretching function. The grid clusters near the inlet and is stretched using a hyperbolic stretching function toward the exit in the streamwise direction. A grid-independence study for smooth pipe flow was performed; Fig. 1 shows the calculated log-law velocity profiles by using both the model of Zhang et al. [42] (denoted as ZH) and the model of Foti and Scandura [46] (denoted as FS) with grids of 91×61, 55×61, and 55×81 in the streamwise and the wall-normal directions, respectively. The Reynolds number, based on the pipe diameter, is 40,000. The experimental data of Laufer [47] are also included for comparison. The computed profiles using the different grids basically collapse for both the ZH and the FS models, indicating that the turbulent flow solutions being grid-independent. The 55×61 grid is used in all the pipe flow solutions presented here. The same grid size is also found to provide grid-independent solutions for channel flows. For the flat-plate boundary flows, Figs. 2 and 3 show the results of the grid-independent study using both models with various grid numbers in the streamwise direction and in the wall-normal direction, respectively. The grid sizes vary widely between 71×150 and

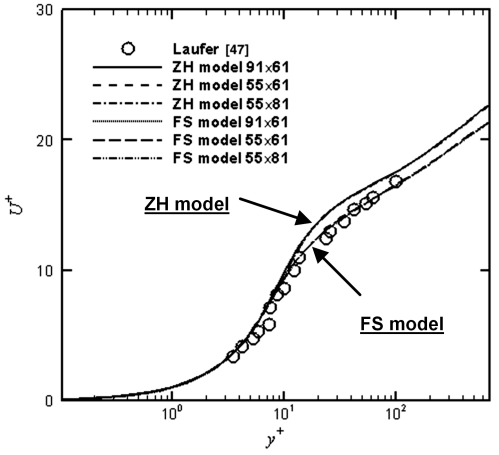

Fig. 1 Grid-independent study with grid refinement in the wall-normal direction.

281 × 150 (Fig. 2) and between 141 × 150 and 141 × 180 (Fig. 3). Figure 2 shows the surface skin friction distributions, which are known to be sensitive to numerical grids, and Fig. 3 shows the computed mean velocity profiles. The results show that, similar to that observed in the pipe flow grid-independence study, the numerical code can achieve grid-independent solutions for the flat-plate turbulent boundary layer. The turbulent flat-plate boundary-layer flow results presented have been obtained by using the 141 × 150 grid.

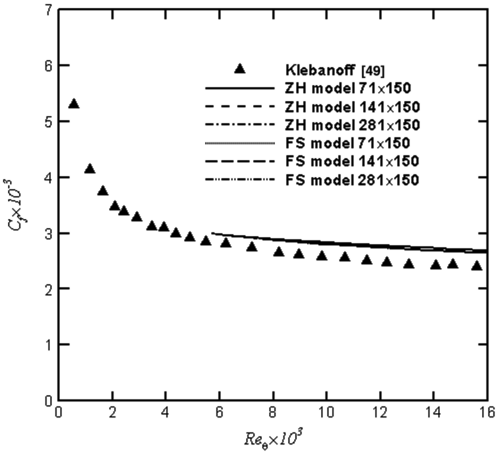

Fig. 2 Grid-independent study for flat plates with grid refinement in the streamwise direction.

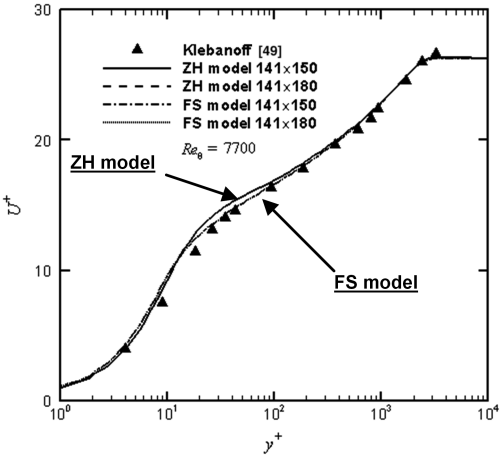

Fig. 3 Grid-independent study for flat plates in the wall-normal direction.

The Courant–Friedrichs–Lewy number used in these computations is 1.5 for the k and ε equations. For all the results shown here, the residuals defined by the summation of differences between the current and the previous iterations were reduced by at least four orders of magnitude.

IV. Results and Discussion

The results of calculations are reported in three sections. The first part presents the results of the application of the two turbulence models to flows in smooth geometries, including pipes, channels, and flat plates. The computational results are compared with measurements and DNS data. The second part compares the computational results for the fully developed rough-pipe and rough-channel flows with the corresponding experimental data. The last part presents numerical investigation of the turbulent boundary layers over flat plates with different types of surface roughness, including uniform spheres, sandpaper, and mesh. The computational results for the skin friction coefficients, the log-law velocity profiles, and the turbulence profiles are presented and compared with the available measurements.

A. Smooth Pipe and Channel Flows and Flat-Plate Turbulent Boundary Layers

The performance of the ZH and the FS models with zero roughness height was evaluated by simulating the fully developed turbulent flows in smooth pipes, in smooth channels, and over smooth flat plates. The FS model with zero roughness height degenerates to the low-Reynolds-number k-ε model of Lam and Bremhorst [43], whereas the ZH model with zero roughness height does not reduce to any existing low-Reynolds-number k-ε models. Figure 1 shows that, compared with the data [47], both models well predict the log-law velocity in the sublayer and outer layer. The present ZH model result was verified with that in Zhang et al. [42] and both results show that the ZH model seems to overpredict in the buffer layer by a maximum of 8%, compared with the measurements. Figure 4, which compares the computed and the measured turbulent kinetic energy profiles, shows that both models overpredict the peak of the turbulent kinetic energy near the wall, yet capture the trends of the experimental data.

The computational results for smooth channel flows have been compared with the DNS data [48] at a Reynolds number, based on channel height, of 13,750 and the results are shown in Fig. 5. Both models nicely predict the log-law velocity in the sublayer and outer layer, whereas the ZH model slightly overpredicts in the buffer layer, compared with the DNS data. The predictions of the turbulent kinetic energy from both models are in good agreement with the DNS data, with a slight underprediction of the peak turbulent kinetic energy near the wall.

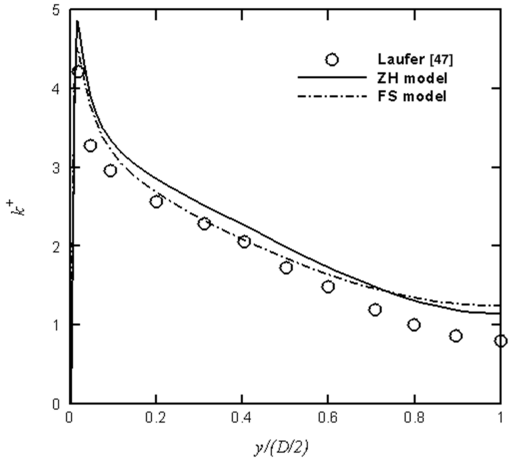

Fig. 4 Comparisons of the turbulent kinetic energy in smooth pipe flows.

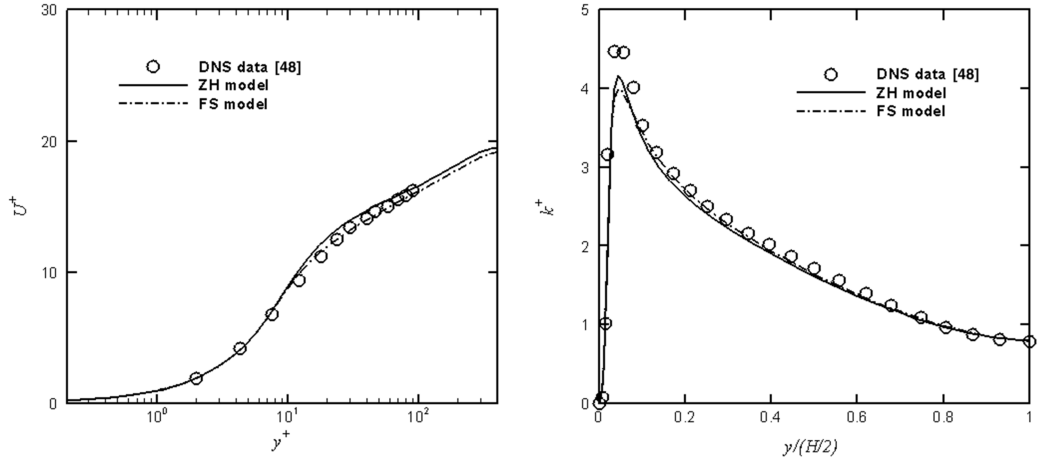

a) b)

Fig. 5 Comparisons of a) the log-law velocity and b) the turbulent kinetic energy in smooth channel flows.

The turbulent boundary-layer flows over smooth plates were also simulated to assess the performance of both models, and the experimental results of Klebanoff [49] for $Re_\theta = 7700$ are used here for comparison. Figure 2 shows that the calculated skin friction coefficients are in good agreement with the experimental data. The computed log-law velocity profiles, as shown in Fig. 3, from both models also agree well with the measurements in the sublayer and outer layer, whereas the ZH model slightly overpredicts the velocity in the buffer layer, compared with the experimental data. The results of the turbulent kinetic energy and the Reynolds shear stress across the boundary layer are shown in Fig. 6. The computational results of the turbulent kinetic energy from both models overpredict the peak of the turbulent kinetic energy near the wall, yet broadly follow the trend of the experimental data. It is also shown in Fig. 6b that both models well predict the Reynolds shear stress in the inner region of $y/\delta < 0.2$ and generally follow the trend of the experimental data in the outer region of $y/\delta > 0.2$.

B. Rough Pipe and Channel Flows

For the fully developed turbulent flows in rough pipes, the comparisons of the calculated roughness function ΔU^+ with the experimental measurements of Prandtl and Schlichting [58] and Colebrook and White [59] in terms of k_{eq}^+ are shown in Fig. 7. In the current calculations, the roughness function ΔU^+ is determined by

$$\Delta U^+ = \left(\sqrt{2/C_f}\right)_{\text{smooth}} - \left(\sqrt{2/C_f}\right)_{\text{rough}} = (U_e/u_\tau)_{\text{smooth}} - (U_e/u_\tau)_{\text{rough}} \tag{18}$$

It can be observed that the ZH model underpredicts the roughness functions ΔU^+ more significantly than that of the FS model. The maximum difference between the predictions and the measurements is 40% for the ZH model, compared with 12% for the FS model.

The ZH and the FS models were also assessed by simulating the fully developed turbulent rough-channel flows measured by Zhang [60] and Bakken et al. [61]. Zhang [60] carried out an experimental study of turbulent flow in a rectangular channel with aspect ratio $W/H = 5.5$, which is covered with 100-grit sandpaper of $k_{\text{eq}}/H =$

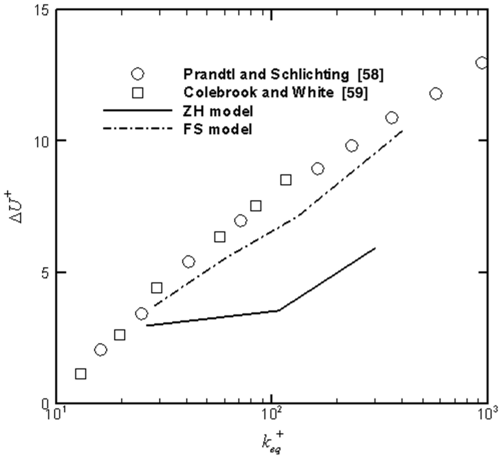

Fig. 7 Comparisons of the roughness functions at various roughness heights in rough-pipe flows.

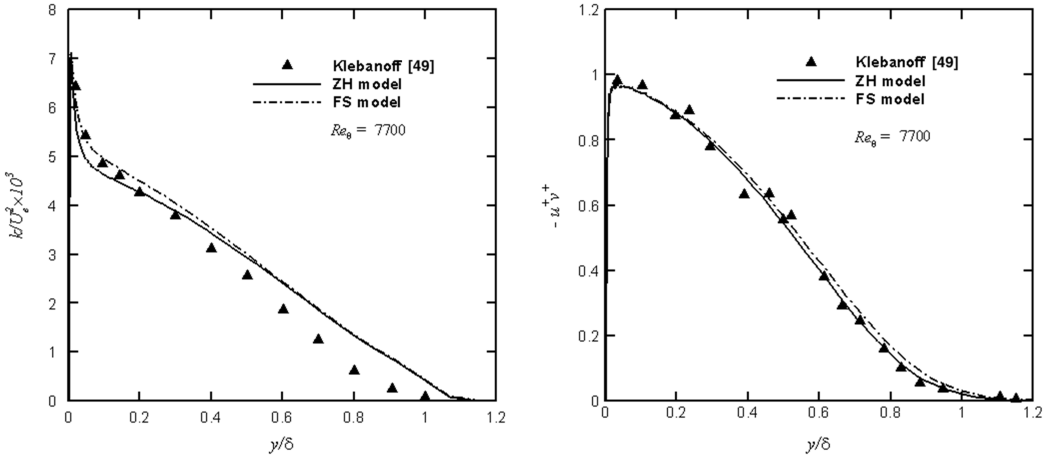

a) b)

Fig. 6 Comparisons of a) the turbulent kinetic energy b) the Reynolds shear stress in flat-plate turbulent boundary layers.

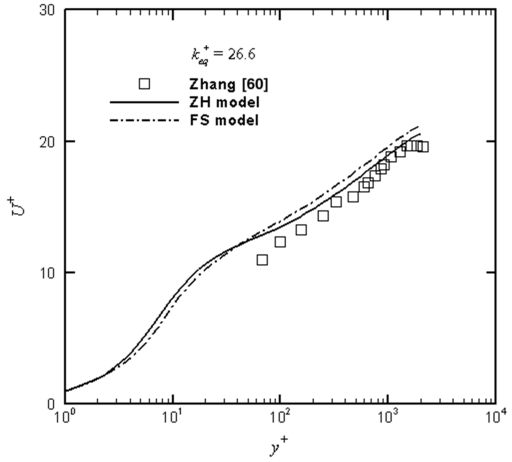

Fig. 8 Comparisons of the log-law velocity in rough-channel flows with roughness of sandpaper.

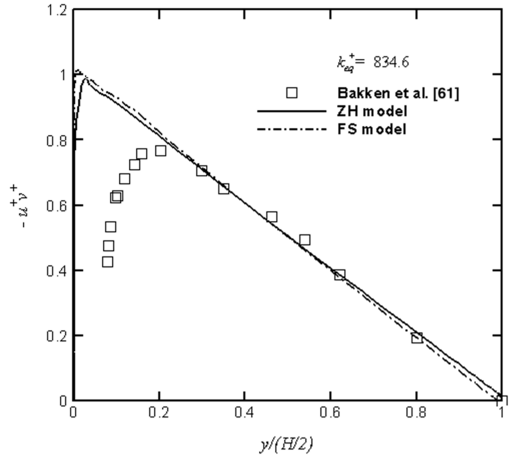

Fig. 10 Comparisons of the Reynolds shear stress in rough-channel flows with rod roughness.

0.0061 at a Reynolds number, based on channel height, of 70,909. Bakken et al. [61] measured turbulent channel flows covered with two different rough surfaces, including a rod of $k_s/H = 0.017$ and mesh of $k_s/H = 0.015$. A range of Reynolds numbers, based on channel height, between 12,000 and 136,000 has been investigated. The results of Bakken et al. [61] show that in the fully rough regime ($k_{eq}^+ > 70$), the ratio k_{eq}/k_s is about 7.8 and 3.3 for the rod and mesh roughness, respectively, indicating a much stronger roughness effect for the rod roughness than for the mesh surface. The computational results of the log-law velocity compared with the experimental measurements of Zhang [60] at $k_{eq}^+ = 26.6$ are presented in Fig. 8. It can be observed that both models have predicted the correct slope, but slightly underpredict the roughness function ΔU^+ (about 7% from the experimental data).

The computational results corresponding to the experiments of Bakken et al. [61] with a Reynolds number, based on channel height, of 60,000 with rod roughness of $k_{eq}^+ = 834.6$ are given in Figs. 9 and 10. For the log-law velocity profile (Fig. 9), both models predict the correct slope, but underpredict the roughness function ΔU^+. It can be also found that the ZH model provides fairly good predictions in the log-law velocity at low roughness k_{eq}^+, yet fails to predict the log-law velocity at high roughness k_{eq}^+. The computational results and the measured data for the Reynolds shear stress are compared in Fig. 10. It is shown that the computed profiles for rod roughness from the ZH and the FS models collapse to the experimental data in the outer region for $y/(H/2) > 0.2$, which is consistent with the wall similarity hypothesis of Townsend [14]. In the inner region of $y/(H/2) < 0.2$, the peak level of the measured Reynolds shear stress profile is lower than the predictions. The reduced peak Reynolds shear stress has been attributed to the local flow acceleration ahead of and above the rod roughness [61].

The comparisons of the roughness function ΔU^+ with the experimental measurements of Prandtl and Schlichting [58] for a wide range of roughness k_{eq}^+ for the fully developed turbulent rough-channel flows are presented in Fig. 11. The FS model well captures the trend of the roughness function variation with the roughness height. However, it underpredicts the roughness function itself. The underprediction of roughness function for the ZH model is significant with a maximum of 38% for higher k_{eq}^+, compared with about 11% for that by the FS model. The ZH model provides good predictions of the log-law velocity for low roughness of $k_{eq}^+ < 30$. Note that the difference between the smooth- and rough-wall ZH models lies in the roughness modeling functions $g_1(k_{eq}^+)$ and $g_2(k_{eq}^+)$. For cases of a smooth wall, $g_1(k_{eq}^+) = 0$ and $g_2(k_{eq}^+) = 1$.

C. Boundary Layers over Rough Flat Plates

The turbulent boundary layers over flat plates with different k-type surface roughness, including mesh [10,13], packed uniform spheres [12], and sandpaper [13], with the roughness k_{eq}^+ of 340, 138, and 100, respectively, were simulated. These experiments were chosen because the measurements were made in the fully rough regime with moderate roughness k_{eq}^+ for several different types of surface roughness.

The comparisons of the computed log-law velocity with that of Antonia and Krogstad [10], which was conducted at a Reynolds number, based on the plate length, of 4.62×10^6 with a mesh screen of $k_s = 1.38$ mm ($k_{eq} = 4.96$ mm) and $k_{eq}^+ = 340$, are provided in Fig. 12. The experimental data were measured at $Re_\theta = 12,800$. It is

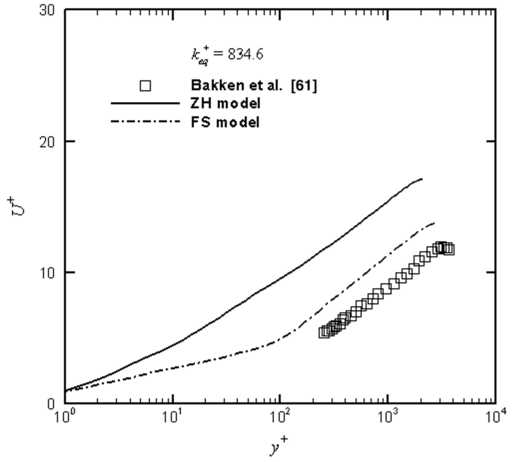

Fig. 9 Comparisons of the log-law velocity in rough-channel flows with rod roughness.

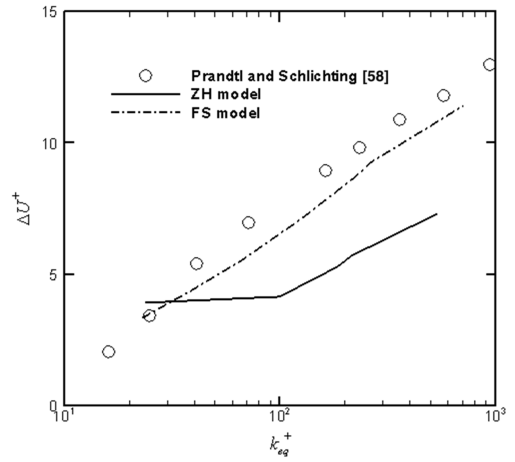

Fig. 11 Comparisons of the roughness functions for a wide range of roughness height in rough-channel flows.

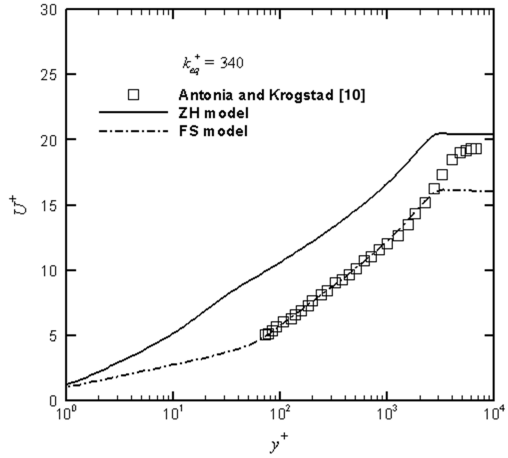

Fig. 12 Comparisons of the log-law velocity at $Re_\theta = 12,800$ in turbulent boundary layer with surface roughness of mesh screen.

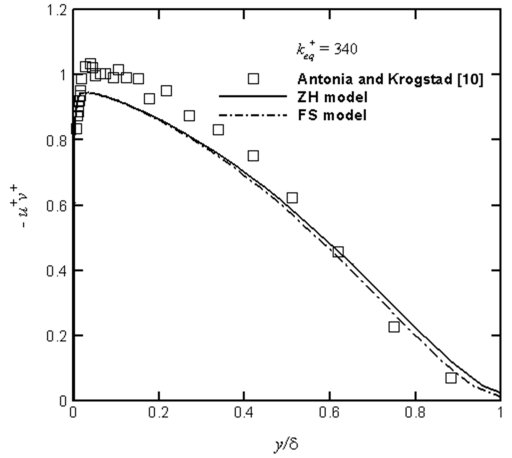

Fig. 14 Comparisons of the Reynolds shear stress at $Re_\theta = 12,800$ in turbulent boundary layer with surface roughness of mesh screen.

shown that the simulation results of the FS model collapse to the experimental data for $y^+ < 2500$. The ZH model predicts the correct slope, but it underpredicts the roughness function ΔU^+ by about 45%, compared with the experimental data. The computed turbulent kinetic energy and the Reynolds shear stress are compared with the experimental measurements, and the comparisons are shown in Figs. 13 and 14, respectively. Figure 13 shows that the computed profiles of k from both models behave similarly for $y/\delta > 0.3$. However, neither model predicts the turbulent kinetic energy distribution in the boundary layer. It is shown in Fig. 14 that the predictions of the Reynolds shear stress from both models are in good agreement with the experimental data in the outer region for $y/\delta > 0.5$ and generally follow the trend of the experimental data.

The second rough-wall turbulent boundary layer that was calculated corresponds to that of Schultz and Flack [12] at a Reynolds number, based on the plate length, of 4.9×10^6 with the roughness of packed uniform spheres of $k_s = k_{\text{eq}} = 0.96 \pm 0.04$ mm and $k_{\text{eq}}^+ = 138$. The experimental study of Schultz and Flack is among the few available experimental measurements that provide the skin friction coefficient data. The computational results of the ZH and the FS models for the skin friction coefficient are compared and the results are presented in Fig. 15. In the experimental study, the skin friction coefficient was calculated using the constant stress method:

$$C_f = \frac{2}{U_e^2}\left[\nu\frac{\partial U}{\partial y} - \overline{uv}\right] \tag{19}$$

whereas in the current calculations, the skin friction coefficient is determined directly from the wall shear stress. That is,

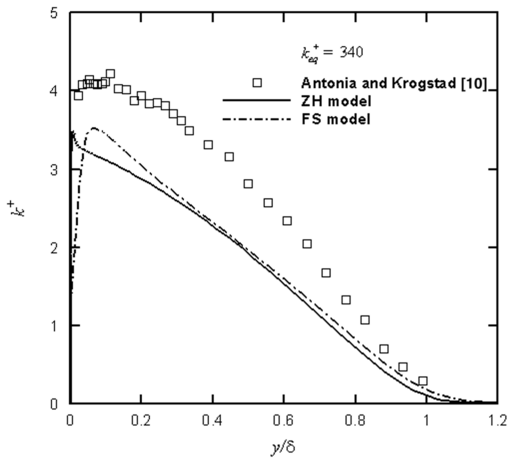

Fig. 13 Comparisons of the turbulent kinetic energy at $Re_\theta = 12,800$ in turbulent boundary layer with surface roughness of mesh screen.

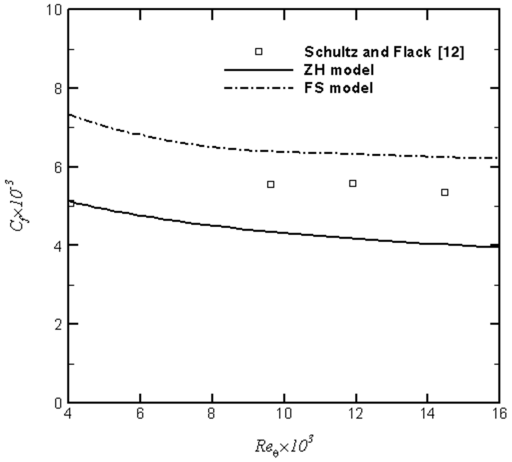

Fig. 15 Predictions of the skin friction coefficients in turbulent boundary layer with surface roughness of uniform spheres.

$$C_f = 2(u_\tau/U_e)^2 \tag{20}$$

It can be observed from Fig. 15 that the FS model overpredicts the skin friction coefficient by about 10%, compared with the experimental data, and the ZH model underpredicts the skin friction coefficient about 18%. The profiles of the log-law velocity and the Reynolds shear stress at $Re_\theta = 9620$ are compared in Figs. 16 and 17, respectively. For the mean velocity, the simulation results of the FS model are in a good agreement with the experimental data in the log-law region, whereas the ZH model predicts the correct slope, yet underpredicts the roughness function by about 42%. The predictions of the Reynolds shear stress from both models are in good agreement with the experimental data, except for the inner region of $y/\delta < 0.2$.

The last set of comparisons for the turbulent boundary layers over rough flat plates is with that of Flack et al. [13] The experimental measurements were carried out with two types of surface roughness. They include sandpaper of $k_s = 0.69$ mm ($k_{\text{eq}} = 0.515$ mm, $k_{\text{eq}}^+ = 100$) and mesh of $k_s = 0.32$ mm ($k_{\text{eq}} = 0.69$ mm and $k_{\text{eq}}^+ = 138$) at a Reynolds number, based on the plate length, of 5.1×10^6. The computational results for the mean velocity and the Reynolds shear stress, compared with the experimental measurements over sandpaper roughness at $Re_\theta = 14,340$, are shown in Figs. 18 and 19, respectively. The mean velocity profile predicted by the FS model collapses with the experimental data for $y^+ < 2500$. The ZH model predicts the correct slope, yet underpredicts the roughness function by 40%, compared with the experimental data. It is shown in Fig. 19 that the predictions of the Reynolds shear stress from both models are in good agreement with the experimental data across the boundary layer. For the mesh roughness and

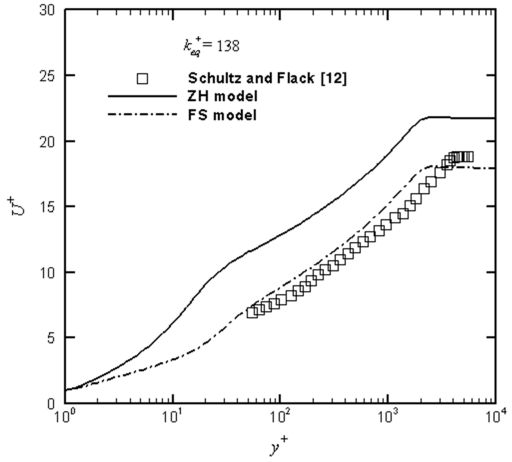

Fig. 16 Comparisons of the log-law velocity at $Re_\theta = 9620$ in turbulent boundary layer with surface roughness of uniform spheres.

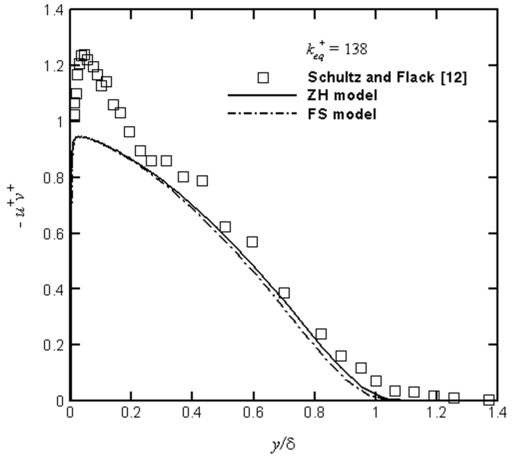

Fig. 17 Comparisons of the Reynolds shear stress at $Re_\theta = 9620$ in turbulent boundary layer with surface roughness of uniform spheres.

$Re_\theta = 14,120$, Figs. 20 and 21 show the computed log-law velocity and the Reynolds shear stress and their comparisons with the experimental measurements. The comparisons show the overall trends being very similar to the case with the sandpaper roughness (Figs. 18 and 19).

The predicted profiles of the Reynolds shear stress using the ZH and the FS models are similar, with peak value around 1.0 at about $y/\delta = 0.05$, and both models describe the Reynolds shear stress

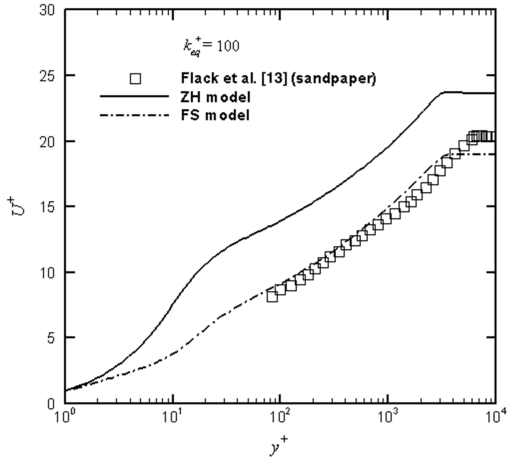

Fig. 18 Comparisons of the log-law velocity at $Re_\theta = 14,340$ in turbulent boundary layer with surface roughness of sandpaper.

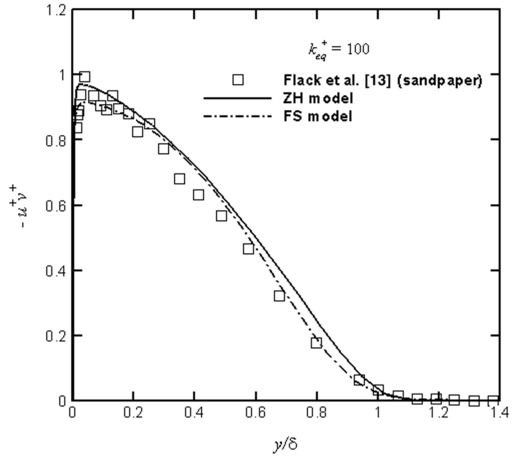

Fig. 19 Comparisons of the Reynolds shear stress at $Re_\theta = 14,340$ in turbulent boundary layer with surface roughness of sandpaper.

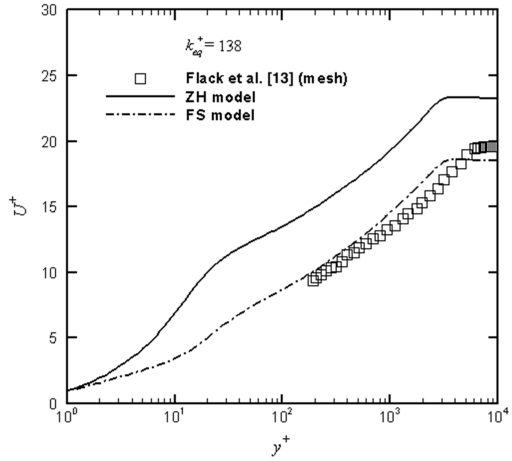

Fig. 20 Comparisons of the log-law velocity at $Re_\theta = 14,120$ in turbulent boundary layer with surface roughness of mesh.

reasonably well across the boundary layer. The computational results of the Reynolds shear stress obtained by using both models also appear to support the wall similarity hypothesis of Townsend [14]. The FS model better reproduces the log-law velocity profiles. Neither model predicts the correct U^+ at the freestream.

Because both models were developed by modifying the damping functions of the existing low-Reynolds-number k-ε models by including the correlated roughness effect through the use of the

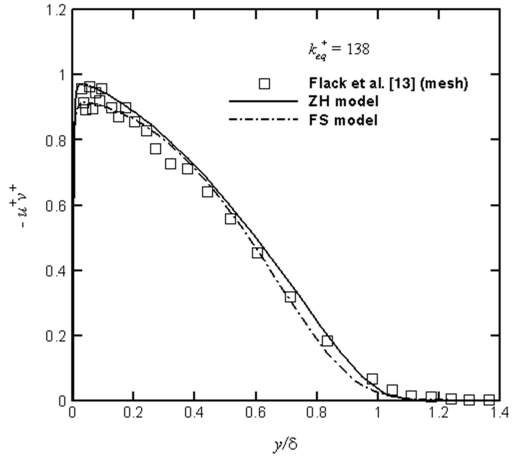

Fig. 21 Comparisons of the Reynolds shear stress at $Re_\theta = 14,120$ in turbulent boundary layer with surface roughness of mesh.

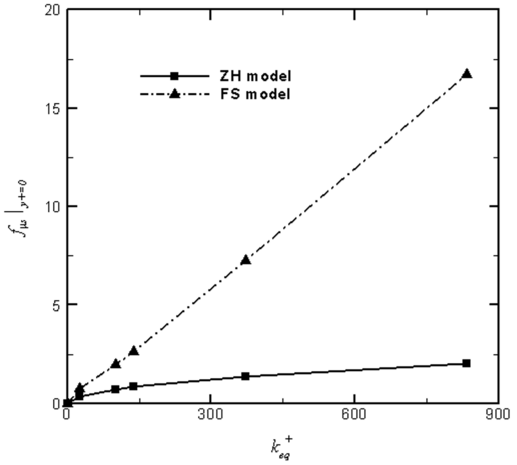

Fig. 22 Comparisons of the two roughness damping functions at the wall.

equivalent sand roughness, we investigated the effect of roughness damping functions $f_{\mu,s}$ in Eqs. (9) and (15) for the range of the roughness k_{eq}^+ used in this study. The comparisons of the two roughness damping functions $f_{\mu,s}$ at $y^+ = 0$ are presented in Fig. 22. It can be observed that as the roughness k_{eq}^+ increases, the roughness damping functions $f_{\mu,s}$ at $y^+ = 0$ for both models increase as well. The difference between the two damping functions $f_{\mu,s}$ at $y^+ = 0$ is not significant for roughness k_{eq}^+ less than 30. For large roughness k_{eq}^+, the values of the wall damping function for both models increase, with the FS model being significantly higher than that for the ZH model. In other words, the ZH model is providing less of an effect of the enhanced turbulent mixing due to roughness than that by the FS model, especially for large roughness k_{eq}^+. This may have caused the observed underprediction of the roughness function for cases with high roughness.

V. Conclusions

The performance of two rough-wall low-Reynolds-number k-ε models was assessed by simulating the fully developed turbulent flow in rough pipes, rough channels, and over rough plates, with the equivalent sand roughness k_{eq}^+ ranging from 26.6 to 834.6. The predictions of the two models are examined against the published experimental measurements. The following remarks can be made based on the results of the comparisons with the experimental data.

1) The model calculations of the fully developed turbulent flows in smooth pipes, smooth channels, and over smooth flat plates agree well with the experimental measurements and the DNS data.

2) The FS model reasonably well predicts the log-law mean velocity profiles and the roughness function ΔU^+ for all of the flows calculated. The predictions of the ZH model of the log-law mean velocity and the roughness function ΔU^+ are satisfactory for low roughness height of $k_{\text{eq}}^+ < 30$.

3) For both models, the predicted Reynolds shear stress profiles with the equivalent sand roughness k_{eq}^+ ranging from 100 to 834.6 agree with the experimental data, except for the inner region $y/(H/2) < 0.2$ of Bakken et al. [61] (channel flow) and the inner region $y/\delta < 0.2$ of Schultz and Flack [12] (flat-plate boundary layer).

4) Both models less satisfactorily predict the skin friction coefficient and the turbulent kinetic energy in the turbulent boundary layers over rough walls.

5) The ZH model does not accurately predict the roughness function ΔU^+ at higher roughness k_{eq}^+, which, when compared with the FS model, may have been caused by the insufficient amount of increase of the damping functions f_μ in the near rough-wall region.

The results of this study, which examines only flows with simple geometries, suggest that there is a need for roughness modeling that can consistently predict the effect of roughness on not only the mean flow, but also the turbulence quantities in the RANS framework. Modeling may be developed that includes consideration of the interactions of the flow structures and roughness. Such physics-based modeling approaches may lead to more consistent and reliable predictions of turbulent flows over roughness.

Acknowledgment

This work was financially supported by the Office of Naval Research and is gratefully acknowledged.

References

[1] Chen, Y.-K., and Milos, F. S., "Ablation and Thermal Response Program for Spacecraft Heatshield Analysis," *Journal of Spacecraft and Rockets*, Vol. 36, No. 3, 1999, pp. 475–483.

[2] Nikuradse, J., "Laws of Flow in Rough Pipes," NACA TM 1292, 1933.

[3] Raupach, M. R., Antonia, R. A., and Rajagopalan, S., "Rough-Wall Turbulent Boundary Layers," *Applied Mechanics Reviews*, Vol. 44, No. 2, 1991, pp. 1–25.

[4] Finnigan, J., "Turbulence in Plant Canopies," *Annual Review of Fluid Mechanics*, Vol. 32, 2000, pp.519–571.

[5] Jimenez, J., "Turbulent Flows over Rough Walls," *Annual Review of Fluid Mechanics*, Vol. 36, 2004, pp. 173–196. doi:10.1146/annurev.fluid.36.050802.122103

[6] Clauser, F. H., "Turbulent Boundary Layers in Adverse Pressure Gradient," *Journal of the Aeronautical Sciences*, Vol. 21, No. 2, 1954, pp. 91–108.

[7] Clauser, F. H., "Turbulent Boundary Layer," *Advances in Applied Mechanics*, Vol. 4, 1956, pp. 1–51.

[8] Hama, F. R., "Boundary-Layer Characteristics for Smooth and Rough Surfaces," *Transactions of the Society of Naval Architecture and Marine Engineers*, Vol. 62, 1954, pp. 333–358.

[9] Perry, A. E., Schofield, W. H., and Joubert, P. N., "Rough Wall Turbulent Boundary Layer," *Journal of Fluid Mechanics*, Vol. 37, No. 2, 1969, pp. 383–413. doi:10.1017/S0022112069000619

[10] Antonia, R. A., and Krogstad, P.-Å., "Turbulence Structure in Boundary Layers over Different Types of Surface Roughness," *Fluid Dynamics Research*, Vol. 28, No. 2, 2001, pp. 139–157. doi:10.1016/S0169-5983(00)00025-3

[11] Schultz, M. P., and Flack, K. A., "Turbulent Boundary Layers over Surfaces Smoothed by Sanding," *Journal of Fluids Engineering*, Vol. 125, No. 5, 2003, pp. 863–870. doi:10.1115/1.1598992

[12] Schultz, M. P., and Flack, K. A., "Outer Layer Similarity in Fully Rough Turbulent Boundary Layers," *Experiments in Fluids*, Vol. 38, No. 3, 2005, pp. 328–340. doi:10.1007/s00348-004-0903-2

[13] Flack, K. A., Schultz, M. P., and Shapiro, T. A., "Experimental Support for Townsend's Reynolds Number Similarity Hypothesis on Rough Walls," *Physics of Fluids*, Vol. 17, No. 3, 2005, pp. 035102-1–035102-9. doi:10.1063/1.1843135

[14] Townsend, A. A., *The Structure of Turbulent Shear Flow*, Cambridge Univ. Press, Cambridge, England, U.K., 1976, p. 139.

[15] Acharya, M., Bornstein, J., and Escudier, M. P., "Turbulent Boundary Layers on Rough Surfaces," *Experiments in Fluids*, Vol. 4, No. 1, 1986, pp. 33–47. doi:10.1007/BF00316784

[16] Krogstad, P.-Å., Antonia, R. A., and Browne, L. W. B., "Comparison Between Rough- and Smooth-Wall Turbulent Boundary Layers," *Journal of Fluid Mechanics*, Vol. 245, 1992, pp. 599–617. doi:10.1017/S0022112092000594

[17] Krogstad, P.-Å., and Antonia, R. A., "Structure of Turbulent Boundary Layers on Smooth and Rough Walls," *Journal of Fluid Mechanics*, Vol. 277, 1994, pp. 1–21. doi:10.1017/S0022112094002661

[18] Krogstad, P.-Å., and Antonia, R. A., "Surface Roughness Effects in Turbulent Boundary Layers," *Experiments in Fluids*, Vol. 27, No. 5, 1999, pp. 450–460. doi:10.1007/s003480050370

[19] Keirsbulck, L., Labraga, L., Mazouz, A., and Tournier, C., "Surface Roughness Effects on Turbulent Boundary Layer Structures," *Journal of Fluids Engineering*, Vol. 124, No. 1, 2002, pp. 127–135. doi:10.1115/1.1445141

[20] Poggi, D., Porporato, A., and Ridolfi, L., "Analysis of the Small-Scale Structure of Turbulence on Smooth and Rough Walls," *Physics of Fluids*, Vol. 15, No. 1, 2003, pp. 35–46. doi:10.1063/1.1521728

[21] Patel, V. C., "Perspective: Flow at High Reynolds Number and over Rough Surface-Achilles Heel of CFD," *Journal of Fluids Engineering*, Vol. 120, 1998, pp. 434–444.

[22] Goddard, F. E., "Effect of Uniformly Distributed Roughness on Turbulent Skin-Friction Drag at Supersonic Speed," *Journal of the Aerospace Sciences*, Vol. 26, 1959, pp. 1–15.

[23] Holden, M. S., "Studies of Surface Roughness and Blowing Effects on Hypersonic Turbulent Boundary Layers over Slender Cones," AIAA Paper 89-0458, 1989.

[24] Fang, Y., Liou, W. W., and Xu, S., "Skin-Friction Prediction for High-Speed Turbulent Boundary Layers with Ablation," *Journal of Spacecraft and Rockets*, Vol. 41, No. 5, 2004, pp. 893–895.

[25] Miyake, Y., Tsujimoto, K., and Agata, Y., "DNS of a Turbulent Flow in a Rough-Wall Channel Using Roughness Elements Model," *JSME International Journal, Series B (Fluids and Thermal Engineering)*, Vol. 43, No. 2, 2000, pp. 233–242.

[26] Miyake, Y., Tsujimoto, K., and Nakaji, M., "Direct Numerical Simulation of Rough-Wall Heat Transfer in a Turbulent Channel Flow," *International Journal of Heat and Fluid Flow*, Vol. 22, No. 3, 2001, pp. 237–244. doi:10.1016/S0142-727X(01)00085-6

[27] Li, A., and Shao, Y., "Numerical Simulation of Drag Partition over Rough Surfaces," *Boundary-Layer Meteorology*, Vol. 108, No. 3, 2003, pp. 317–342. doi:10.1023/A:1024179025508

[28] Scotti, A., "Direct Numerical Simulation of Turbulent Channel Flows with Boundary Roughened with Virtual Sandpaper," *Physics of Fluids*, Vol. 18, No. 3, 2006, pp. 031701. doi:10.1063/1.2183806

[29] Goldstein, D., Handler, R., and Sirovich, L., "Direct Numerical Simulation of Turbulent Flow over a Modelled Riblet Covered Surface," *Journal of Fluid Mechanics*, Vol. 302, 1995, pp. 333–376. doi:10.1017/S0022112095004125

[30] Lee, C., "Large-Eddy Simulation of Rough-Wall Turbulent Boundary Layers," *AIAA Journal*, Vol. 40, No. 10, 2002, pp. 2127–2130.

[31] Cui, J., Patel, V. C., and Lin, C., "Prediction of Turbulent Flow over Rough Surfaces Using a Force Field in Large Eddy Simulation," *Journal of Fluids Engineering*, Vol. 125, No. 1, 2003, pp. 2–9. doi:10.1115/1.1524587

[32] Bhaganagar, K., Kim, J., and Coleman, G., "Effect Of Roughness On Wall-Bounded Turbulence," *Flow, Turbulence and Combustion*, Vol. 72, Nos. 2–4, Special Issue, 2004, pp. 463–492. doi:10.1023/B:APPL.0000044407.34121.64

[33] Taylor, R. P., Coleman, H. W., and Hodge, B. K., "Prediction of Turbulent Rough-Wall Skin Friction Using a Discrete Element Approach," *Journal of Fluids Engineering*, Vol. 107, No. 2, 1985, pp. 251–257.

[34] Taylor, R. P., Scaggs, W. F., and Coleman, H. W., "Measurement and Prediction of the Effects of Nonuniform Surface Roughness on Turbulent Flow Friction Coefficients," *Journal of Fluids Engineering*, Vol. 110, 1988, pp. 380–384.

[35] Taylor, R. P., Hodge, B. K., and Coleman, H. W., "Discrete Element Model for Turbulent Skin Friction Prediction for Rib-Type Surface Roughness," *Heat and technology*, Vol. 7, No. 1, 1989, pp. 29–48.

[36] Tarada, F., "Prediction of Rough-Wall Boundary Layers Using a Low Reynolds Number k-ε Model," *International Journal of Heat and Fluid Flow*, Vol. 11, No. 4, 1990, pp. 331–345. doi:10.1016/0142-727X(90)90057-I

[37] Maruyama, T., "Surface and Inlet Boundary Conditions for the Simulation of Turbulent Boundary Layer over Complex Rough Surfaces," *Journal of Wind Engineering and Industrial Aerodynamics*, Vol. 81, No. 1, May 1999, pp. 311–322. doi:10.1016/S0167-6105(99)00026-4

[38] Yamamoto, M., "Proposal of a Rans Model to Predict Both k- and d-Type Roughness," *Proceedings of the 4th ASME/JSME Joint Fluids Engineering Conference*, Vol. 1, Pt. C, American Society of Mechanical Engineers, New York, 2003, pp. 2019–2024.

[39] Krogstad, P.-Å., "Modification of the Van Driest Damping Function to Include the Effects of Surface Roughness," *AIAA Journal*, Vol. 29, No. 6, 1991, pp. 888–894.

[40] Van Driest, E. R., "On Turbulent Flow near a Wall," *Journal of Aerospace Science*, Vol. 23, No. 11, 1956, pp. 1007–1011.

[41] Youn, B., Yuen, C., and Mills, A. F., "Friction Factor for Flow in Rectangular Ducts with One Side Rib-Roughened," *Journal of Fluids Engineering*, Vol. 116, No. 3, 1994, pp. 488–493.

[42] Zhang, H., Faghri, M., and White, F. M., "New Low-Reynolds-Number k-ε Model for Turbulent Flow over Smooth and Rough Surfaces," *Journal of Fluids Engineering*, Vol. 118, No. 2, 1996, pp. 255–259.

[43] Lam, C. K. G., and Bremhorst, K., "A Modified Form of the k-ε Model for Predicting Wall Turbulence," *Journal of Fluids Engineering*, Vol. 103, No. 3, 1981, pp. 456–460.

[44] Durbin, P. A., Medic, G., Seo, J.-M., Eaton, J. K., and Song, S., "Rough Wall Modification of Two-Layer k-ε," *Journal of Fluids Engineering*, Vol. 123, No. 1, Mar. 2001, pp. 16–21. doi:10.1115/1.1343086

[45] Chen, H. C., and Patel, V. C., "Near-Wall Turbulence Models for Complex Flows Including Separation," *AIAA Journal*, Vol. 26, No. 6, 1988, pp. 641–648.

[46] Foti, E., and Scandura, P., "A Low Reynolds Number k-ε Model Validated for Oscillatory Flows over Smooth and Rough Walls," *Coastal Engineering*, Vol. 51, No. 2, 2004, pp. 173–184. doi:10.1016/j.coastaleng.2004.01.001

[47] Laufer, J., "The Structure of Turbulence in Fully Developed Pipe Flow," NACA TM 1174, 1952.

[48] Mansour, N. N., Kim, J., and Moin, P., "Reynolds Stress and Dissipation Rate Budgets in Turbulent Channel Flow," *Journal of Fluid Mechanics*, Vol. 194, Sept. 1988, pp. 15–44. doi:10.1017/S0022112088002885

[49] Klebanoff, P. S., "Characteristic of Turbulence in a Boundary Layer with Zero Pressure Gradient," NACA TM1247, 1954.

[50] Ligrani, P. M., and Moffat, R. J., "Structure of Transitionally Rough and Fully Rough Turbulent Boundary Layers," *Journal of Fluid Mechanics*, Vol. 162, Jan. 1986, pp. 69–98. doi:10.1017/S0022112086001933

[51] Sotiropoulos, F., and Abdallah, S., "The Discrete Continuity Equation in Primitive Variable Solutions of Incompressible Flow," *Journal of Computational Physics*, Vol. 95, July 1991, pp. 212–227. doi:10.1016/0021-9991(91)90260-R

[52] Sotiropoulos, F., and Patel, V. C., "Flow in Curved Ducts of Varying Cross-Section," Iowa Institute of Hydraulic Research, Rept. 358, Iowa City, IA, 1992.

[53] Sinha, S. K., Sotiropouslos, F., and Odgaard, A. J., "Three-Dimensional Numerical Model for Flows Through Natural Rivers," *Journal of Hydraulic Engineering*, Vol. 124, 1998, pp. 13–24. doi:10.1061/(ASCE)0733-9429(1998)124:1(13)

[54] Lu, M., and Sirviente, A. I., "Numerical Study of the Momentumless Wake of an Axisymmetric Body," *43rd AIAA Aerospace Sciences Meeting and Exhibit—Meeting Papers*, AIAA, Reston, VA, 2005, pp. 10175–10188.

[55] Kim, K., Sirviente, A. I., and Beck, R. F., "The Complementary RANS Equations for the Simulation of Viscous Flows," *International Journal for Numerical Methods in Fluids*, Vol. 48, No. 2, 2005, pp. 199–229. doi:10.1002/fld.892

[56] Yaras, M. I., and Grosvenor, A. D., "Evaluation of One- and Two-Equation Low-*Re* Turbulence Models, Part 1: Axisymmetric Separating and Swirling Flows," *International Journal for Numerical Methods in Fluids*, Vol. 42, No. 12, 2003, pp. 1293–1319. doi:10.1002/fld.585

[57] Patel, V. C., Rodi, W., and Scheuerer, G., "Turbulence Models for Near-Wall and Low Reynolds Number Flows: A Review," *AIAA Journal*, Vol. 23, No. 9, 1985, pp. 1308–1319.

[58] Prandtl, L., and Schlichting, H., "Das Wiederstandagesetz Rouher Platten," *Werft-Reederei-Hafen*, Vol. 15, 1934, pp. 1–4.

[59] Colebrook, C. M., and White, C. M., "Experiments with Fluid Motion in Roughened Pipes," *Proceedings of the Royal Society of London A*, Vol. 161, 1937, pp. 367–381. doi:10.1098/rspa.1937.0150

[60] Zhang, H., "Study of a Numerical Turbulence Model for Flow Past Smooth and Rough Surfaces," Ph.D. Dissertation, Department of Mechanical Engineering, Univ. of Rhode Island, Kingston, RI, 1993.

[61] Bakken, O. M., Krogstad, P.-Å., Ashrafian, A., and Andersson, H. I., "Reynolds Number Effects in the Outer Layer of the Turbulent Flow in a Channel with Rough Walls," *Physics of Fluids*, Vol. 17, No. 6, 2005, p. 065101. doi:10.1063/1.1900146

R. Kimmel
Associate Editor